

# Landau gauge gluon and ghost propagators from lattice QCD with $N_f = 2$ twisted mass fermions at finite temperature

R. Aouane,<sup>1</sup> F. Burger,<sup>1</sup> E.-M. Ilgenfritz,<sup>1,2</sup> M. Müller-Preussker,<sup>1</sup> and A. Sternbeck<sup>3</sup>

<sup>1</sup>*Humboldt-Universität zu Berlin, Institut für Physik, 12489 Berlin, Germany*

<sup>2</sup>*Joint Institute for Nuclear Research, VBLHEP, 141980 Dubna, Russia*

<sup>3</sup>*Universität Regensburg, Institut für Theoretische Physik, 93040 Regensburg, Germany*

(Dated: March 13, 2013)

We investigate the temperature dependence of the Landau gauge gluon and ghost propagators in lattice QCD with two flavors of maximally twisted mass fermions. For these propagators we provide and analyze data which corresponds to pion mass values between 300 and 500 MeV. For the gluon propagator we find that both the longitudinal and transversal component change smoothly in the crossover region, while the ghost propagator exhibits only a very weak temperature dependence. For momenta between 0.4 and 3.0 GeV we give a parametrization for our lattice data. It may serve as input to studies which employ continuum functional methods.

PACS numbers: 11.15.Ha, 12.38.Gc, 12.38.Aw

Keywords: Lattice QCD, finite temperature, Landau gauge, gluon and ghost propagators

## I. INTRODUCTION

Hadronic matter may experience a phase transition or crossover from a confined phase, with broken chiral symmetry, to a deconfined chirally symmetric phase. The latter phase is characterized by a state called *quark gluon plasma*. It is widely believed this state of matter has been passed in the early universe, and efforts are undertaken to reproduce it experimentally in heavy-ion collisions as in present collider experiments at RHIC (BNL) or with the ALICE and CMS detectors at LHC (CERN).

The possible existence of such a phase transition was first discussed [1] in the context of Hagedorn's thermodynamic model [2, 3] as a way to evade the consequence of a maximal hadronic temperature. First numerical evidence has been found already in the early days of lattice QCD (LQCD) [4, 5]. In fact, the lattice formulation offers an ab-initio approach to study such aspects of QCD nonperturbatively. This remains true as long as the chemical potential is small compared to the temperature. Over the last decade immense computational resources were dedicated to reach at a consistent picture of QCD at finite temperature and zero chemical potential (for recent reviews see [6–9]).

LQCD, however, is not the only framework to tackle nonperturbative problems of QCD at zero or non-zero temperature. Powerful continuum functional methods exist as well, like for instance in the context of Dyson-Schwinger (DS) equations [10–13] or functional renormalization group (FRG) equations [14–16], which also allow to address such problems.

Within these frameworks (see, e.g., the recent reviews [17, 18]) the Landau gluon and ghost propagators appear—together with the corresponding vertices—as the main building blocks in the formulation of the DS or FRG equations; they constitute part of the solutions of the latter. These functional methods though come with a potential source of error: To solve the (infinite)

tower of equations it has to be truncated appropriately, and so the solutions beyond the far-infrared regime, depend on how the truncations are done, in particular in the momentum range around  $O(1)$  GeV. Therefore, independent information, at best from first principles, is welcome to improve these (unavoidable) truncations.

LQCD calculations allow to provide the Landau gluon and ghost propagators in an ab-initio way. The available momentum range, however, is restricted from above by the lattice spacing and from below by the available lattice volume (up to a further uncertainty related to so-called Gribov copies [19, 20]). Despite these restrictions, an impressive amount of data has been produced over the last years for these propagators at zero (see, e.g., [21, 22] and references therein) and non-zero temperature [20, 21, 23–36]. This data has allowed for a variety of cross-checks with corresponding results from the continuum functional methods.

Conventional lattice calculations of QCD at finite temperature often employ the Polyakov loop and the chiral condensate to probe for the (de)confinement and chiral phase transition, respectively. In recent years it turned out that these and other observables can be also calculated from DS and FRG equations, where the Landau gauge gluon and ghost propagators are used as input [30, 37–43]. Even an extrapolation to the notoriously difficult regime of nonzero chemical potential seems to be possible [44, 45]. Appropriate lattice data for the propagators close to the continuum limit is therefore essential to assist those efforts.

In a recent study [33] we have provided such data for quenched QCD (see, e.g., [46] for a first application). We could show that the longitudinal (electric) component of the gluon propagator may be used to probe the thermal phase transition of pure  $SU(3)$  gauge theory. Similar was shown in [34]. The present article further complements the available lattice data with finite-temperature data for the Landau gauge gluon and ghost propagators from LQCD with  $N_f = 2$  dynamical fermion flavors. To the

best of our knowledge, there are only two studies which have provided such data in the past [31, 47].

For our study we adopt a lattice formulation that employs the Symanzik-improved gauge action for the gluonic field and the twisted mass Wilson-fermion action for the fermionic part. The latter ensures an automatic  $O(a)$  improvement provided the Wilson  $\kappa$ -parameter is tuned to maximal twist (for further details we refer to [48, 49]). Our data is based on the vast set of gauge field configurations that has been generated by the tmfT Collaboration. The tmfT Collaboration has explored the complicated phase structure of the theory [50] and is still investigating the smooth crossover region from the confining and chirally broken regime at low temperature  $T$  to the deconfinement and chirally restored phase at high  $T$  [51, 52]. These studies are restricted so far to pseudo-scalar meson (pion) masses from 300 MeV to 500 MeV. To set the scale we use results at  $T = 0$  of the European Twisted Mass (ETM) Collaboration [53]. Specifically, our data for the gluon and ghost propagators covers the whole crossover regime at three pion mass values:  $m_\pi \simeq 316, 398$  and  $469$  MeV. At these values the crossover regime is characterized by a very smooth behavior of the chiral condensate and the Polyakov loop as well as their susceptibilities. Moreover, one observes for these settings the breakdown of chiral symmetry and the deconfinement phase transition occur at slightly different temperatures  $T_c = T_\chi$  and  $T_{\text{deconf}}$ , respectively, in agreement with observations reported in [54].<sup>1</sup>

The paper is organized as follows. In Section II we give all lattice parameters and outline the setup of our Monte Carlo simulations. Section III recalls the definitions of the gluon and ghost propagators on the lattice in the Landau gauge. Data and fits for various temperature and pion mass values are presented in Section IV. Conclusions are drawn in Section V.

## II. LATTICE ACTION AND SIMULATION PARAMETERS

Our study is based on gauge field configurations provided by the tmfT Collaboration. These configurations were generated on a four-dimensional periodic lattice of spatial linear size  $N_\sigma = 32$  and a temporal extent of  $N_\tau = 12$  for a mass-degenerate doublet of twisted mass fermions, cf. the review in Ref. [48]. The corresponding gauge action is the tree-level Symanzik improved action

defined as

$$S_G = \beta \sum_x \left[ c_0 \sum_{\mu < \nu} \left( 1 - \frac{1}{3} \Re \text{Tr} U_{x\mu\nu}^{1 \times 1} \right) + c_1 \sum_{\mu \neq \nu} \left( 1 - \frac{1}{3} \Re \text{Tr} U_{x\mu\nu}^{1 \times 2} \right) \right], \quad (1)$$

with  $\beta = 2N_c/g_0^2$ ,  $c_1 = -\frac{1}{12}$ ,  $c_0 = 1 - 8c_1$  and  $g_0$  being the bare coupling constant.  $U_{x\mu\nu}^{1 \times 1}$  represents quadratic and  $U_{x\mu\nu}^{1 \times 2}$  rectangular Wilson loops built from the link variables  $U_{x\mu} \in SU(3)$ . One important feature of this gauge action is its inherent  $O(a)$  improvement. For more details see Refs. [55, 56]. The Wilson fermion action with an additional parity-flavor symmetry violating improvement term reads [57]

$$S_F[U, \psi, \bar{\psi}] = \sum_x \bar{\chi}(x) (1 - \kappa D_W[U] + 2i\kappa a \mu_0 \gamma_5 \tau_3) \chi(x), \quad (3)$$

where the Pauli matrix  $\tau_3$  acts in flavor space and the fermionic fields are expressed in terms of the twisted basis  $\{\bar{\chi}, \chi\}$ , which is related to the physical fields  $\{\bar{\psi}, \psi\}$  by

$$\psi = \frac{1}{\sqrt{2}}(1 + i\gamma_5 \tau_3)\chi \quad \text{and} \quad \bar{\psi} = \bar{\chi} \frac{1}{\sqrt{2}}(1 + i\gamma_5 \tau_3). \quad (4)$$

The Wilson covariant derivative acts on these as

$$D_W[U]\psi(x) = \sum_\mu ((r - \gamma_\mu)U_\mu(x)\psi(x + \hat{\mu}) + (r + \gamma_\mu)U_\mu^\dagger(x - \hat{\mu})\psi(x - \hat{\mu})), \quad (5)$$

and the quark mass is set by the twisted mass parameter  $\mu_0$  and the hopping parameter  $\kappa = (2am_0 + 8r)^{-1}$ , parameterizing the untwisted bare quark mass component. Here  $a$  is the lattice spacing and  $r = 1$ . Note that for any finite  $\beta$  the value for  $\kappa$  gets corrections through mass renormalization.

It must be noted that maximal twist is accomplished by tuning the hopping parameter to its critical value  $\kappa_c$ , where the untwisted theory would become massless. At maximal twist one achieves an automatic  $O(a)$ -improved fermion formulation [58]. The hopping parameter entering the simulation is based on a set of  $\beta$ -values for which  $\kappa_c(\beta)$  was provided by the ETM Collaboration [53]. For intermediate  $\beta$  the corresponding  $\kappa_c$  values are obtained through an interpolation as described in Ref. [52]. The bare twisted mass parameter  $a\mu_0$  has been adjusted such as to keep the physical pion mass constant along our scans in the bare inverse coupling  $\beta$ .

As usual in finite temperature QCD, the imaginary time extent  $N_\tau$  corresponds to the inverse temperature  $T^{-1} = N_\tau a(\beta)$ . To quote it in physical units we use interpolated—as well as slightly extrapolated—data for the lattice spacing reported for  $\beta = 3.90, 4.05$  and  $4.20$

<sup>1</sup> Detailed results are presented in a recent update to [52]. We thank the tmfT Collaboration for providing us their  $T_c$ -data prior to publication.

by the ETM Collaboration [53] (see also Ref. [52]). We restrict our analysis to lattice spacings  $a < 0.09$  fm.

For the reader's convenience all parameters, like  $\beta$ , the corresponding lattice spacings, temperatures, pion masses, the number of independent configurations and other relevant values are collected in Table I. Note that there, for definiteness, "pion mass" corresponds to the charged pion. In Table II we provide also the respective pseudo-critical couplings  $\beta_c$  and the corresponding temperatures  $T_\chi$  and  $T_{\text{deconf}}$  for the three pion mass values we use. These temperatures were obtained from fits around the maxima of the chiral susceptibility  $\sigma_{\psi\psi}^2$ , and from the behavior of the (renormalized) Polyakov loop  $\langle \mathfrak{R}\epsilon(L) \rangle_R$ , respectively (see the revised version of Ref. [52]).

### III. THE GLUON AND GHOST PROPAGATORS ON THE LATTICE

Glueon and ghost propagators are gauge dependent quantities. As in Ref. [33] we focus on Landau gauge and therefore have to transform the (unfixed) tmfT gauge ensemble until it satisfies the corresponding gauge condition. In differential form it reads

$$\nabla_\mu A_\mu = \sum_{\mu=1}^4 (A_\mu(x + \hat{\mu}/2) - A_\mu(x - \hat{\mu}/2)) = 0 \quad (6)$$

with the lattice gauge potentials

$$A_\mu(x + \hat{\mu}/2) = \frac{1}{2ia g_0} (U_{x\mu} - U_{x\mu}^\dagger) |_{\text{traceless}}. \quad (7)$$

To render the link variables satisfying this condition one maximizes the gauge functional

$$F_U[g] = \frac{1}{3} \sum_{x,\mu} \mathfrak{R}\epsilon \text{Tr} (g_x^\dagger U_{x\mu} g_{x+\mu}) \quad (8)$$

by successive local gauge transformations  $g_x$  acting on the link variables as follows

$$U_{x\mu} \xrightarrow{g} U_{x\mu}^g = g_x^\dagger U_{x\mu} g_{x+\mu}, \quad g_x \in SU(3). \quad (9)$$

In order to achieve this, we subsequently apply two methods, first simulated annealing (*SA*) and then over-relaxation (*OR*). *OR* is applied to finally satisfy the gauge condition (Eq. (6)) with a local accuracy of

$$\max_x \mathfrak{R}\epsilon \text{Tr} [\nabla_\mu A_{x\mu} \nabla_\nu A_{x\nu}^\dagger] < 10^{-13}, \quad (10)$$

while *SA* to reduce the Gribov ambiguity of lattice Landau gauge, by favoring gauge-fixed (Gribov) copies with large values for  $F_U[g]$ , see [21, 22, 60–65]. For this the *SA* algorithm generates gauge transformations  $\{g_x\}$  randomly by a Monte Carlo chain with a statistical weight  $\sim \exp(F_U[g]/T_{sa})$ . The "simulated annealing temperature"  $T_{sa}$  is a technical parameter which is monotonously lowered. Our annealing schedule is specified by a hot

start at  $T_{sa} = 0.45$ , after which  $T_{sa}$  is continuously lowered in equal steps until  $T_{sa} = 0.01$  is reached. We apply 3500 *SA* steps between these two temperatures, and, for better performance, also added a few microcanonical steps to each (heatbath) step. Since we apply large number of *SA* steps to maximize  $F_U[g]$ , we restrict ourselves to one Gribov copy per configuration.

Our first quantity of interest is the gluon propagator defined in momentum space as the ensemble average

$$D_{\mu\nu}^{ab}(q) = \langle \tilde{A}_\mu^a(k) \tilde{A}_\nu^b(-k) \rangle, \quad (11)$$

where  $\langle \dots \rangle$  represents the average over configurations.  $\tilde{A}_\mu^a(k)$  denotes the Fourier transform of the gauge potential (7) and  $k_\mu \in (-N_\mu/2, N_\mu/2]$  is the lattice momentum ( $\mu = 1, \dots, 4$ ), which relates to the physical momentum  $q_\mu$  as

$$q_\mu(k_\mu) = \frac{2}{a} \sin\left(\frac{\pi k_\mu}{N_\mu}\right). \quad (12)$$

Henceforth we will use the notation  $(N_\sigma; N_\tau) \equiv (N_i; N_4)$  where  $i = 1, 2, 3$ .

For non-zero temperature Euclidean invariance is broken, and it is useful to split  $D_{\mu\nu}^{ab}(q)$  into two components, the transversal  $D_T$  ("chromomagnetic") and the longitudinal  $D_L$  ("chromoelectric") propagator, respectively,

$$D_{\mu\nu}^{ab}(q) = \delta^{ab} (P_{\mu\nu}^T D_T(q_4^2, \vec{q}^2) + P_{\mu\nu}^L D_L(q_4^2, \vec{q}^2)). \quad (13)$$

The fourth momentum component  $q_4$  conjugate to the Euclidean time (Matsubara frequency) will be restricted to zero later on. For Landau gauge  $P_{\mu\nu}^{T,L}$  represent projectors transversal and longitudinal relative to the time-direction ( $\mu = 4$ ):

$$P_{\mu\nu}^T = (1 - \delta_{\mu 4})(1 - \delta_{\nu 4}) \left( \delta_{\mu\nu} - \frac{q_\mu q_\nu}{\vec{q}^2} \right), \quad (14)$$

$$P_{\mu\nu}^L = \left( \delta_{\mu\nu} - \frac{q_\mu q_\nu}{\vec{q}^2} \right) - P_{\mu\nu}^T. \quad (15)$$

For the propagators  $D_{T,L}$  [or their respective dimensionless dressing functions  $Z_{T,L}(q) = q^2 D_{T,L}(q)$ ] we find

$$D_T(q) = \frac{1}{2N_g} \left\langle \sum_{i=1}^3 \tilde{A}_i^a(k) \tilde{A}_i^a(-k) - \frac{q_4^2}{\vec{q}^2} \tilde{A}_4^a(k) \tilde{A}_4^a(-k) \right\rangle \quad (16)$$

and

$$D_L(q) = \frac{1}{N_g} \left( 1 + \frac{q_4^2}{\vec{q}^2} \right) \langle \tilde{A}_4^a(k) \tilde{A}_4^a(-k) \rangle, \quad (17)$$

where  $N_g = N_c^2 - 1$  and  $N_c = 3$ . The zero-momentum propagator values are then defined as

$$D_T(0) = \frac{1}{3N_g} \sum_{i=1}^3 \langle \tilde{A}_i^a(0) \tilde{A}_i^a(0) \rangle, \quad (18)$$

$$D_L(0) = \frac{1}{N_g} \langle \tilde{A}_4^a(0) \tilde{A}_4^a(0) \rangle. \quad (19)$$

$m_\pi$ [MeV]	$T$ [MeV]	$a$ [fm]	$r_0/a$	$r_0 \cdot T$	$n_{conf}$	$\beta$	$\kappa_c(\beta)$	$a \cdot \mu_0(\beta)$	$\tilde{Z}_T$	$\tilde{Z}_L$	$\tilde{Z}_J$
316(16)	187	$8.77(47) \cdot 10^{-2}$	4.81	0.40	293	3.8400	0.162731	0.00391	0.6380(80)	0.6264(108)	0.66862(32)
316(16)	199	$8.25(22) \cdot 10^{-2}$	5.17	0.43	299	3.8800	0.161457	0.00360	0.6208(34)	0.6139(50)	0.66939(10)
316(16)	215	$7.65(13) \cdot 10^{-2}$	5.63	0.47	255	3.9300	0.159998	0.00346	0.6117(70)	0.6116(103)	0.67264(14)
316(16)	222	$7.39(12) \cdot 10^{-2}$	5.84	0.49	273	3.9525	0.159385	0.00335	0.6156(59)	0.6122(84)	0.67252(15)
316(16)	225	$7.31(12) \cdot 10^{-2}$	5.91	0.49	151	3.9600	0.159187	0.00331	0.6151(71)	0.6101(102)	
316(16)	228	$7.22(11) \cdot 10^{-2}$	5.98	0.50	250	3.9675	0.158991	0.00328	0.6120(63)	0.6079(114)	0.67388(14)
316(16)	230	$7.14(11) \cdot 10^{-2}$	6.05	0.50	113	3.9750	0.158798	0.00325	0.6146(77)	0.5982(126)	
316(16)	235	$6.98(11) \cdot 10^{-2}$	6.19	0.52	290	3.9900	0.158421	0.00319	0.6092(71)	0.6118(97)	0.67536(14)
398(16)	193	$8.51(32) \cdot 10^{-2}$	4.99	0.42	159	3.8600	0.162081	0.00617	0.6191(64)	0.6147(98)	0.66730(21)
398(16)	199	$8.25(22) \cdot 10^{-2}$	5.17	0.43	173	3.8800	0.161457	0.00600	0.6202(54)	0.6192(76)	
398(16)	215	$7.65(13) \cdot 10^{-2}$	5.63	0.47	209	3.9300	0.159998	0.00561	0.6076(59)	0.6080(84)	0.67005(23)
398(16)	228	$7.20(11) \cdot 10^{-2}$	6.00	0.50	198	3.9700	0.158927	0.00531	0.6087(59)	0.6119(89)	
398(20)	236	$6.98(11) \cdot 10^{-2}$	6.19	0.52	156	3.9900	0.158421	0.00517	0.6075(139)	0.6090(231)	0.67293(13)
398(16)	241	$6.82(10) \cdot 10^{-2}$	6.34	0.53	150	4.0050	0.158053	0.00506	0.6156(87)	0.6112(115)	0.6784(60)
398(20)	246	$6.69(10) \cdot 10^{-2}$	6.46	0.54	271	4.0175	0.157755	0.00498	0.6036(78)	0.6063(101)	0.67504(16)
398(20)	248	$6.62(10) \cdot 10^{-2}$	6.53	0.54	226	4.0250	0.157579	0.00493	0.6001(64)	0.6005(94)	0.67517(11)
398(20)	254	$6.47(10) \cdot 10^{-2}$	6.68	0.56	113	4.0400	0.157235	0.00483	0.6029(119)	0.6167(178)	0.67519(26)
469(24)	222	$7.42(12) \cdot 10^{-2}$	5.81	0.48	146	3.9500	0.159452	0.00779	0.6121(55)	0.6020(82)	0.67142(16)
469(24)	228	$7.20(11) \cdot 10^{-2}$	6.00	0.50	348	3.9700	0.158926	0.00752	0.6116(80)	0.6024(110)	0.67128(14)
469(24)	235	$6.98(11) \cdot 10^{-2}$	6.19	0.52	120	3.9900	0.158421	0.00738	0.6098(70)	0.6041(102)	0.67271(22)
469(24)	243	$6.77(10) \cdot 10^{-2}$	6.39	0.53	210	4.0100	0.157933	0.00718	0.6086(54)	0.6093(73)	0.67322(12)
469(24)	247	$6.67(10) \cdot 10^{-2}$	6.48	0.54	250	4.0200	0.157696	0.00708	0.5947(54)	0.5927(77)	0.67147(14)
469(24)	250	$6.57(10) \cdot 10^{-2}$	6.58	0.55	256	4.0300	0.157463	0.00699	0.6013(72)	0.6017(101)	0.67388(14)
469(24)	254	$6.47(10) \cdot 10^{-2}$	6.68	0.56	152	4.0400	0.157235	0.00689	0.6033(80)	0.6028(121)	0.67353(16)
469(24)	258	$6.38(10) \cdot 10^{-2}$	6.78	0.56	150	4.0500	0.157010	0.00680	0.5971(62)	0.6072(91)	0.67485(17)
469(24)	266	$6.19(12) \cdot 10^{-2}$	6.98	0.58	200	4.0700	0.156573	0.00662	0.5972(143)	0.6119(195)	0.67829(32)

TABLE I: The pion mass values, the temperature  $T$ , both in MeV, the lattice spacing  $a$  in fm, the chirally extrapolated Sommer scale  $r_0$  [59],  $r_0 T$ , and the number  $n_{conf}$  of independent configurations used for the analysis are shown in the left subtable for all simulation ensembles.

In the central subtable the values of the inverse bare coupling  $\beta$  used in the simulations, the critical hopping parameter  $\kappa_c$  and the bare twisted mass  $\mu_0$  are additionally shown. The spatial ( $N_\sigma = 32$ ) and temporal ( $N_\tau = 12$ ) sizes are the same for all ensembles. The number  $n_{copy}$  of gauge copies was fixed to 1.

In the right subtable the renormalization factors for the transverse and longitudinal gluon as well as for the ghost dressing function denoted by  $\tilde{Z}_T$ ,  $\tilde{Z}_L$  and  $\tilde{Z}_J$ , respectively (see the text), are given for the renormalization scale  $\mu = 2.5$  GeV.

tmfT ensemble	A12	B12	C12
$m_\pi$ [MeV]	316(16)	398(20)	469(24)
$\beta_c$ from $\sigma_{\psi\psi}^2$	3.89(3)	3.93(2)	3.97(3)
$T_\chi$ [MeV]	202(7)	217(5)	229(5)
$\beta_c$ from $\langle \Re(L) \rangle_R$	-	4.027(14)	4.050(15)
$T_{deconf}$ [MeV]	-	249(5)	258(5)

TABLE II: Extracted (pseudo-) critical couplings  $\beta_c$  and the crossover-temperatures  $T_\chi$  and  $T_{deconf}$  for the three ensembles A12, B12, and C12. Corresponding pion masses (from [52]) are listed in the first row. Ensemble names indicate  $N_\tau = 12$ .

Note that we have neglected a possible  $O(a)$  improvement related to the use of the improved gauge action Eq. (1).

The Landau gauge ghost propagator is given by

$$\begin{aligned}
G^{ab}(q) &= a^2 \sum_{x,y} \langle e^{-2\pi i(k/N) \cdot (x-y)} [M^{-1}]_{xy}^{ab} \rangle \\
&= \delta^{ab} G(q) = \delta^{ab} J(q)/q^2, \quad (20)
\end{aligned}$$

where the four-vector  $(k/N) \equiv (k_\mu/N_\mu)$ .  $J(q)$  denotes the ghost dressing function. The matrix  $M$  is the lattice

Faddeev-Popov operator

$$M_{xy}^{ab} = \sum_{\mu} [A_{x,y}^{ab} \delta_{x,y} - B_{x,y}^{ab} \delta_{x+\hat{\mu},y} - C_{x,\mu}^{ab} \delta_{x-\hat{\mu},y}] \quad (21)$$

with

$$\begin{aligned}
A_{x,y}^{ab} &= \Re \text{Tr} \{ [T^a, T^b] (U_{x,\mu} + U_{x-\hat{\mu},\mu}) \}, \\
B_{x,y}^{ab} &= 2 \cdot \Re \text{Tr} [T^b T^a U_{x,\mu}], \\
C_{x,y}^{ab} &= 2 \cdot \Re \text{Tr} [T^a T^b U_{x-\hat{\mu},\mu}],
\end{aligned}$$

written in terms of  $T^a$ ,  $a = 1, \dots, N_g$ , i.e. the Hermitian generators of the  $su(3)$  Lie algebra normalized according to  $\text{Tr}[T^a T^b] = \delta^{ab}/2$ . For the inversion of  $M$  we use the pre-conditioned conjugate gradient algorithm of [63] with plane-wave sources  $\tilde{\psi}_c^a$  with color and position components  $\psi_c^a(x) = \delta_c^a \exp(2\pi i k \cdot (x/N))$ .

To reduce lattice artifacts, we apply cylinder and cone cuts to our data [66]. Specifically we consider only diagonal and slightly off-diagonal momenta for the gluon propagator and diagonal momenta for the ghost propagator. Moreover, only modes with zero Matsubara frequency ( $k_4 = 0$ ) are used.

## IV. GLUON AND GHOST PROPAGATOR RESULTS

### A. Momentum dependence

Data for the unrenormalized transverse ( $Z_T$ ) and longitudinal ( $Z_L$ ) gluon dressing functions and also for the ghost dressing function ( $J$ ) is shown in Fig. 1. We show it versus the physical momentum  $q \equiv |\vec{q}|$  for selected temperatures and for three pion masses (panels from top to bottom are for  $m_\pi \simeq 316, 398$  and  $469$  MeV, respectively). The corresponding renormalized functions, in momentum subtraction (MOM) schemes, can be obtained from

$$\begin{aligned} Z_{T,L}^{ren}(q, \mu) &\equiv \tilde{Z}_{T,L}(\mu) Z_{T,L}(q), \\ J^{ren}(q, \mu) &\equiv \tilde{Z}_J(\mu) J(q) \end{aligned} \quad (22)$$

with the  $\tilde{Z}$ -factors being defined such that  $Z_{T,L}^{ren}(\mu, \mu) = J^{ren}(\mu, \mu) = 1$ . For a renormalization scale of  $\mu = 2.5$  GeV the  $\tilde{Z}$ -factors are quoted in Table I.

Fig. 1 also shows curves connecting data points of same temperature. These were obtained from fits to the data for momenta  $0.4 \text{ GeV} \leq q \leq 3.0 \text{ GeV}$ . These curves may serve as input to studies of the corresponding DS or FRG equations.

More specifically, for the gluon dressing function we employed (analogously to our quenched study [33]) the Gribov-Stingl formula [67, 68]

$$Z_{\text{fit}}(q) = q^2 \frac{c(1 + dq^{2n})}{(q^2 + r^2)^2 + b^2}, \quad (23)$$

which has been also used in [32, 69] and appears in the context of the so-called ‘‘Refined Gribov-Zwanziger’’ framework [70, 71]. But we found it sufficient to set  $b^2 = 0$  and  $n = 1$ . This fits well the data for  $q \in [0.4, 3.0]$  GeV and gives excellent  $\chi_{dof}^2$  values. The latter together with the results for the fit parameters are listed in Table III. Note again that Fig. 1 shows data and the corresponding fits only for a selected range of temperatures, but Table III gives the fit parameters for all available temperatures. We cannot exclude that the  $b^2$ -term is needed for smaller momenta. If true, it would indicate the occurrence of a pair of complex-conjugate poles.

For momenta above 3 GeV the fit fails to describe the data. In this range logarithmic corrections are expected to become important.

For the ghost dressing function we propose to use a fit formula like

$$J_{\text{fit}}(q) = \left( \frac{f^2}{q^2} \right)^k + h \quad (24)$$

In a first attempt we also tried  $hq^2/(q^2 + m_{gh}^2)$  for the last term with  $m_{gh}$  as a free parameter, but this was always found being consistent with  $m_{gh} = 0$ . We therefore omit such infrared mass parameter and only keep a constant term  $h$  in the ultraviolet limit.

Fit results for the fitting range  $[0.4 \text{ GeV}, 4.0 \text{ GeV}]$  are presented also in Table III. One notes that our  $\chi_{dof}^2$  values are far from being optimal, in particular for the lower temperatures. Deviations typically occur at the lowest momenta. But this could not be cured, e.g., by a mass term  $m_{gh}^2$  alone. However note, the maximal deviations of fit and data points do not exceed 5%.

### B. Temperature dependence

We now look at the temperature dependence of the dressing functions, where our temperature values cover the chiral restoration and the deconfinement phase transition, with the latter being signaled by a peak in the Polyakov loop susceptibility. These two crossover phenomena typically occur at different temperatures and will be denoted  $T_\chi$  and  $T_{\text{deconf}}$ , respectively, in what follows (see Table II for their values).

Looking once again at Fig. 1, we see that the momentum dependences of  $Z_L(q)$  and  $Z_T(q)$  change differently with temperature, irrespective of  $m_\pi$ . In fact, while the (unrenormalized) transverse dressing function  $Z_T$  seems to be relatively insensitive to the temperature, the curves describing  $Z_L(q)$  fan out for momenta below the renormalization scale  $\mu = 2.5$  GeV. A stronger temperature dependence we also observed for  $D_L(q)$  for pure  $SU(3)$  gauge theory [33], though there it was found to be much more pronounced due to the existence of a first order phase transition [33].

These observations are seen more clearly in Fig. 2, where we show ratios of the renormalized dressing functions or propagators

$$R_{T,L}(q, T) = D_{T,L}^{ren}(q, T) / D_{T,L}^{ren}(q, T_{\text{min}}), \quad (25)$$

$$R_G(q, T) = G^{ren}(q, T) / G^{ren}(q, T_{\text{min}}) \quad (26)$$

as functions of the temperature  $T$  for 6 fixed (interpolated) momentum values  $q \neq 0$ , and for different pion masses (panels from top to bottom). For better visibility, ratios are normalized with respect to the respective left-most shown temperature in Fig. 2.

Looking at Fig. 2, we see  $R_L(q, T)$  decrease more or less monotonously with temperature in the crossover region, and this decrease is stronger the smaller the momentum.  $R_T(q, T)$  instead signals a slight increase within the same range, and the ghost propagator (at fixed low momenta) seems to rise a bit around  $T \simeq T_{\text{deconf}}$ .

Fig. 2 does not show ratios at zero momentum, but we show it for  $R_T$  in Fig. 3 (upper row), again versus  $T$  and from left to right for different pion masses. For  $m_\pi \approx 398$  MeV, for example,  $R_T(0, T)$  clearly rises towards  $T_{\text{deconf}}$ , whereas there are only weak indications for such a behavior for  $R_T(0, T)$  for the other two data sets. Much more statistics is necessary to resolve that.

The lower panels of Fig. 3, show data for the inverse renormalized longitudinal propagator  $D_L^{ren}$  at zero momentum, again versus temperature and from left to right

$\beta$	$Z_T$ fits				$Z_L$ fits				$Z_J$ fits			
	$c/a^2$	$d/a^2$	$a r$	$\chi_{dof}^2$	$c/a^2$	$d/a^2$	$a r$	$\chi_{dof}^2$	$a^2 f^2$	$h/a^2$	$k$	$\chi_{dof}^2$
3.8400	1.868(142)	0.420(78)	0.510(12)	0.13	1.334(132)	0.744(138)	0.415(14)	0.19	0.4580(17)	1.0916(61)	0.5111(78)	0.69
3.8800	1.729(60)	0.463(40)	0.486(5)	0.66	1.183(59)	0.872(79)	0.390(7)	0.16	0.41822(7)	1.0904(19)	0.4950(23)	8.59
3.9300	1.371(104)	0.647(111)	0.431(10)	0.36	1.032(101)	1.013(188)	0.370(13)	0.12	0.37046(9)	1.1355(39)	0.5438(55)	2.29
3.9525	1.218(76)	0.757(96)	0.411(8)	0.22	1.049(93)	0.941(159)	0.370(11)	0.16	0.35672(9)	1.1387(36)	0.5462(52)	2.40
3.9600	1.208(88)	0.744(122)	0.405(10)	0.05	0.932(103)	1.148(233)	0.355(14)	0.13				
3.9675	1.256(83)	0.682(107)	0.410(9)	0.10	1.023(108)	0.979(206)	0.369(13)	0.27	0.34636(7)	1.1501(33)	0.5642(54)	5.20
3.9750	1.099(93)	0.852(156)	0.387(11)	0.07	0.938(119)	1.165(277)	0.359(15)	0.09				
3.9900	0.982(70)	1.026(143)	0.369(9)	0.38	0.914(98)	1.143(224)	0.358(13)	0.38	0.33093(8)	1.1571(30)	0.5736(56)	7.01
3.8600	1.811(109)	0.459(66)	0.501(9)	0.32	1.271(116)	0.799(143)	0.401(13)	0.19	0.4464(21)	1.0419(40)	0.4444(35)	31.1
3.8800	1.637(88)	0.523(63)	0.477(8)	0.66	1.218(83)	0.808(107)	0.391(9)	0.11				
3.9300	1.389(84)	0.651(86)	0.437(8)	0.37	0.982(91)	1.092(177)	0.356(12)	0.11	0.3802(19)	1.0962(53)	0.4945(58)	21.4
3.9700	1.151(71)	0.819(110)	0.397(8)	0.48	1.034(86)	0.928(160)	0.366(10)	0.67				
3.9900	1.035(171)	0.965(310)	0.383(21)	0.25	1.171(265)	0.699(430)	0.383(42)	0.21	0.3380(07)	1.1466(25)	0.5612(39)	24.0
4.0050	1.092(104)	0.784(162)	0.381(12)	0.25	1.006(145)	0.924(281)	0.366(19)	0.15	0.441(84)	0.90(14)	0.41(06)	0.21
4.0175	1.035(87)	0.891(164)	0.373(10)	0.44	0.922(133)	1.087(297)	0.356(18)	0.12	0.3189(09)	1.1623(31)	0.5834(60)	6.4
4.0250	1.020(78)	0.904(144)	0.368(9)	0.21	0.845(94)	1.278(270)	0.346(13)	0.11	0.3155(08)	1.1630(25)	0.5853(52)	17.4
4.0400	0.837(111)	1.237(329)	0.340(15)	0.12	0.824(173)	1.252(502)	0.348(24)	0.08	0.3135(21)	1.2200(90)	0.696(21)	0.93
3.9500	1.338(80)	0.645(89)	0.427(8)	0.63	0.952(78)	1.127(169)	0.348(10)	0.35	0.3621(09)	1.1325(38)	0.5397(53)	2.3
3.9700	1.290(104)	0.648(127)	0.416(11)	0.14	0.993(100)	1.003(199)	0.351(12)	0.32	0.3519(07)	1.1426(31)	0.5554(48)	4.2
3.9900	1.126(91)	0.797(139)	0.389(10)	0.28	0.883(96)	1.203(236)	0.343(13)	0.19	0.3405(12)	1.1555(45)	0.5787(81)	2.3
4.0100	1.009(61)	0.937(115)	0.371(7)	0.32	0.998(82)	0.945(157)	0.368(10)	0.23	0.3295(07)	1.1607(24)	0.5873(48)	13.1
4.0200	1.027(67)	0.946(124)	0.375(8)	0.07	1.010(80)	0.918(156)	0.356(9)	1.08	0.3270(08)	1.1557(27)	0.5778(51)	7.0
4.0300	1.096(79)	0.775(135)	0.380(9)	0.48	0.900(87)	1.108(223)	0.349(11)	0.67	0.3130(08)	1.1538(26)	0.5660(48)	7.9
4.0400	0.941(84)	1.018(191)	0.359(11)	0.22	0.870(103)	1.131(275)	0.340(14)	0.25	0.3100(11)	1.2015(55)	0.648(12)	2.3
4.0500	1.053(69)	0.781(126)	0.367(8)	0.67	0.826(89)	1.251(260)	0.344(13)	0.25	0.3082(11)	1.2109(51)	0.677(12)	0.94
4.0700	0.792(130)	1.291(405)	0.328(34)	0.15	0.971(250)	0.894(559)	0.371(32)	0.01	0.2913(20)	1.2156(79)	0.682(19)	0.39

TABLE III: Results from fits with the Gribov-Stingl formula Eq. (23) for the unrenormalized  $Z_T$  (left subtable) and  $Z_L$  (center subtable) gluon dressing functions. The fit range is  $[0.4 : 3.0]$  GeV. The values in parentheses indicate the fit errors estimated with the bootstrap method. The parameters  $b$  and  $n$  were fixed to  $b = 0$  and  $n = 1$ , respectively.

Fit results for the unrenormalized ghost dressing function  $Z_J$  with the fitting function according to Eq. (24) are presented in the right subtable. The momentum fitting ranges are here  $[0.4 : 4.0]$  GeV. The pion mass values are  $m_\pi = 316(16)$  MeV (upper),  $m_\pi = 398(20)$  MeV (middle) and  $m_\pi = 469(24)$  MeV (bottom subtables), respectively.

for different pion masses. This quantity can be identified with an infrared gluon screening mass, and we clearly see it to rise with temperature in the crossover region. This again shows that this infrared gluon screening mass may serve as an useful indicator for the finite-temperature crossover of the quark-gluon system. However, we should keep in mind that the zero-momentum results for the gluon propagators are influenced also by strong finite-size and Gribov copy effects, which we could not analyze here.

## V. CONCLUSION

We have presented data for the Landau gauge gluon and ghost propagators for lattice QCD at finite temperature with  $N_f = 2$  twisted mass fermion flavors. Our data is for a momentum range of 0.4 GeV to 4.0 GeV and was obtained on gauge field configurations produced by the tmFT Collaboration. This has allowed us to explore the propagator's momentum dependence over the whole temperature range of the crossover region, and this separately for three (charged) pion mass values between

300 MeV and 500 MeV. We find that the propagators change smoothly passing through the crossover region and the most significant change is seen for the longitudinal (i.e., electric) component of the gluon propagator.

We also provide fitting functions for our data. These and the corresponding fit parameters, given in Table III, may serve as interpolation functions of our data when used as input to studies which employ continuum functional methods to address problems of QCD at finite temperature. Actually, for both the transversal and longitudinal gluon dressing function these interpolation functions give quite a good description of our data for all temperatures. For the ghost dressing function, this is achieved only for selected temperatures (see Table III for details).

We hope our results will help these (continuum-based) studies to get further predictions of the behavior of hadronic matter close to the transition region that would be too difficult if addressed on the lattice directly.

## Acknowledgments

We thank the members of the tmfT Collaboration for giving us access to their gauge field configurations produced for  $N_f = 2$  fermion degrees of freedom with the Wilson-twisted mass approach. We express our gratitude to the HLRN supercomputer centers in Berlin and Han-

nover for generous supply with computing time. R. A. expresses thanks to L. Zeidlewicz for his help in carrying out the data analysis and gratefully acknowledges financial support by the Yousef Jameel Foundation. A. S. acknowledges support from the European Reintegration Grant (FP7-PEOPLE-2009-RG No.256594), and F. B. from the DFG-funded graduate school GK 1504.

- 
- [1] N. Cabibbo and G. Parisi, Phys.Lett. **B59**, 67 (1975).  
 [2] R. Hagedorn, Nuovo Cim. **A56**, 1027 (1968).  
 [3] R. Hagedorn, Nucl.Phys. **B24**, 93 (1970).  
 [4] L. D. McLerran and B. Svetitsky, Phys.Lett. **B98**, 195 (1981).  
 [5] J. Kuti, J. Polonyi, and K. Szlachanyi, Phys.Lett. **B98**, 199 (1981).  
 [6] K. Kanaya, PoS **Lat2010**, 012 (2010), 1012.4247.  
 [7] L. Levkova, PoS **LATTICE2011**, 011 (2011), 1201.1516.  
 [8] O. Philipsen (2012), 1207.5999.  
 [9] M. P. Lombardo, Plenary talk given at Lattice 2012, to appear in PoS **LATTICE2012** (2012).  
 [10] L. von Smekal, A. Hauck, and R. Alkofer, Ann. Phys. **267**, 1 (1998), hep-ph/9707327.  
 [11] A. Hauck, L. von Smekal, and R. Alkofer, Comput.Phys.Commun. **112**, 166 (1998), hep-ph/9804376.  
 [12] C. D. Roberts and S. M. Schmidt, Prog.Part.Nucl.Phys. **45**, S1 (2000), nucl-th/0005064.  
 [13] P. Maris and C. D. Roberts, Int.J.Mod.Phys. **E12**, 297 (2003), nucl-th/0301049.  
 [14] H. Gies, Phys.Rev. **D66**, 025006 (2002), hep-th/0202207.  
 [15] J. M. Pawłowski, D. F. Litim, S. Nedelko, and L. von Smekal, Phys. Rev. Lett. **93**, 152002 (2004), hep-th/0312324.  
 [16] J. Braun, L. M. Haas, F. Marhauser, and J. M. Pawłowski, Phys. Rev. Lett. **106**, 022002 (2011), 0908.0008 [hep-ph].  
 [17] C. S. Fischer, A. Maas, and J. M. Pawłowski, Annals Phys. **324**, 2408 (2009), 0810.1987.  
 [18] P. Boucaud, J. Leroy, A. L. Yaouanc, J. Micheli, O. Pene, et al. (2011), 1109.1936.  
 [19] V. G. Bornyakov, V. K. Mitrjushkin, and M. Müller-Preussker, Phys. Rev. **D79**, 074504 (2009), 0812.2761.  
 [20] V. Bornyakov and V. Mitrjushkin (2010), 1011.4790.  
 [21] V. G. Bornyakov, V. K. Mitrjushkin, and M. Müller-Preussker, Phys. Rev. **D81**, 054503 (2010), 0912.4475.  
 [22] I. L. Bogolubsky, E.-M. Ilgenfritz, M. Müller-Preussker, and A. Sternbeck, Phys. Lett. **B676**, 69 (2009), 0901.0736.  
 [23] U. M. Heller, F. Karsch, and J. Rank, Phys. Lett. **B355**, 511 (1995), hep-lat/9505016.  
 [24] U. M. Heller, F. Karsch, and J. Rank, Phys. Rev. **D57**, 1438 (1998), hep-lat/9710033.  
 [25] A. Cucchieri, F. Karsch, and P. Petreczky, Phys. Lett. **B497**, 80 (2001), hep-lat/0004027.  
 [26] A. Cucchieri, F. Karsch, and P. Petreczky, Phys. Rev. **D64**, 036001 (2001), hep-lat/0103009.  
 [27] A. Cucchieri, A. Maas, and T. Mendes, Phys. Rev. **D75**, 076003 (2007), hep-lat/0702022.  
 [28] R. Sousa, M. Chiapparini, A. Cucchieri, and T. Mendes, Int.J.Mod.Phys. **E16**, 2939 (2007).  
 [29] A. Maas, Chin. J. Phys. **34**, 1328 (2010), 0911.0348.  
 [30] C. S. Fischer, A. Maas, and J. A. Mueller, Eur. Phys. J. **C68**, 165 (2010), 1003.1960.  
 [31] V. G. Bornyakov and V. K. Mitrjushkin (2011), 1103.0442.  
 [32] A. Cucchieri and T. Mendes (2011), 1105.0176.  
 [33] R. Aouane, V. Bornyakov, E. Ilgenfritz, V. Mitrjushkin, M. Müller-Preussker, and A. Sternbeck, Phys.Rev. **D85**, 034501 (2012), 1108.1735.  
 [34] A. Maas, J. M. Pawłowski, L. von Smekal, and D. Spielmann, Phys.Rev. **D85**, 034037 (2012), 1110.6340.  
 [35] A. Cucchieri and T. Mendes, PoS **LATTICE2011**, 206 (2011), 1201.6086.  
 [36] A. Cucchieri, D. Dudal, T. Mendes, and N. Vandersickel (2012), 1202.0639.  
 [37] J. Braun, H. Gies, and J. M. Pawłowski, Phys. Lett. **B684**, 262 (2010), 0708.2413.  
 [38] C. S. Fischer, A. Maas, and J. M. Pawłowski, PoS **CONFINEMENT8**, 043 (2008), 0812.2745.  
 [39] C. S. Fischer, Phys.Rev.Lett. **103**, 052003 (2009), 0904.2700.  
 [40] C. S. Fischer and J. A. Mueller, Phys.Rev. **D84**, 054013 (2011), 1106.2700.  
 [41] C. S. Fischer and J. Luecker (2012), 1206.5191.  
 [42] L. Fister and J. M. Pawłowski (2011), 1112.5429.  
 [43] L. Fister and J. M. Pawłowski (2011), 1112.5440.  
 [44] C. S. Fischer, J. Luecker, and J. A. Mueller, Phys.Lett. **B702**, 438 (2011), 1104.1564.  
 [45] J. Luecker and C. S. Fischer, Prog.Part.Nucl.Phys. **67**, 200 (2012), 1111.0180.  
 [46] K. Fukushima and K. Kashiwa (2012), 1206.0685.  
 [47] S. Furui and H. Nakajima, Phys. Rev. **D76**, 054509 (2007), hep-lat/0612009.  
 [48] A. Shindler, Phys. Rept. **461**, 37 (2008), 0707.4093.  
 [49] C. Urbach, PoS **LATTICE 2007**, 022 (2007), arXiv:0710.1517 [hep-lat].  
 [50] E.-M. Ilgenfritz, K. Jansen, M. Lombardo, M. Müller-Preussker, M. Petschlies, O. Philipsen, and L. Zeidlewicz, Phys.Rev. **D80**, 094502 (2009), 0905.3112.  
 [51] F. Burger, E.-M. Ilgenfritz, M. Kirchner, M. Lombardo, M. Müller-Preussker, O. Philipsen, C. Urbach, and L. Zeidlewicz (tmfT collaboration), PoS (**LAT2010**) **220** (2010), 1009.3758.  
 [52] F. Burger, E.-M. Ilgenfritz, M. Kirchner, M. Lombardo, M. Müller-Preussker, O. Philipsen, C. Urbach, and L. Zeidlewicz (tmfT collaboration) (2011), 1102.4530.  
 [53] R. Baron et al. (ETM), JHEP **08**, 097 (2010), 0911.5061.  
 [54] S. Borsanyi et al. (Wuppertal-Budapest), JHEP **09**, 073 (2010), 1005.3508.  
 [55] K. Symanzik, Nucl. Phys. **B226**, 187 (1983).  
 [56] K. Symanzik, Nucl. Phys. **B226**, 205 (1983).  
 [57] R. Frezzotti, P. A. Grassi, S. Sint, and P. Weisz (Alpha),

- JHEP **08**, 058 (2001), [hep-lat/0101001].
- [58] R. Frezzotti and G. Rossi, JHEP **0408**, 007 (2004), hep-lat/0306014.
- [59] R. Sommer, Nucl. Phys. **B411**, 839 (1994), hep-lat/9310022.
- [60] C. Parrinello and G. Jona-Lasinio, Phys. Lett. **B251**, 175 (1990).
- [61] D. Zwanziger, Nucl. Phys. **B345**, 461 (1990).
- [62] T. D. Bakeev, E.-M. Ilgenfritz, V. K. Mitrjushkin, and M. Müller-Preussker, Phys. Rev. **D69**, 074507 (2004), hep-lat/0311041.
- [63] A. Sternbeck, E.-M. Ilgenfritz, M. Müller-Preussker, and A. Schiller, Phys. Rev. **D72**, 014507 (2005), hep-lat/0506007.
- [64] I. L. Bogolubsky, G. Burgio, V. K. Mitrjushkin, and M. Müller-Preussker, Phys. Rev. **D74**, 034503 (2006), hep-lat/0511056.
- [65] I. L. Bogolubsky, V. G. Bornyakov, G. Burgio, E.-M. Ilgenfritz, V. K. Mitrjushkin, and M. Müller-Preussker, Phys. Rev. **D77**, 014504 (2008), 0707.3611.
- [66] D. B. Leinweber, J. I. Skullerud, A. G. Williams, and C. Parrinello (UKQCD), Phys. Rev. **D60**, 094507 (1999), hep-lat/9811027.
- [67] V. N. Gribov, Nucl. Phys. **B139**, 1 (1978).
- [68] M. Stingl, Z.Phys. **A353**, 423 (1996), hep-th/9502157.
- [69] A. Cucchieri, T. Mendes, and A. R. Taurines, Phys.Rev. **D67**, 091502 (2003), hep-lat/0302022.
- [70] D. Dudal, J. A. Gracey, S. P. Sorella, N. Vandersickel, and H. Verschelde, Phys. Rev. **D78**, 065047 (2008), 0806.4348.
- [71] D. Dudal, S. Sorella, and N. Vandersickel, Phys.Rev. **D84**, 065039 (2011), 1105.3371.



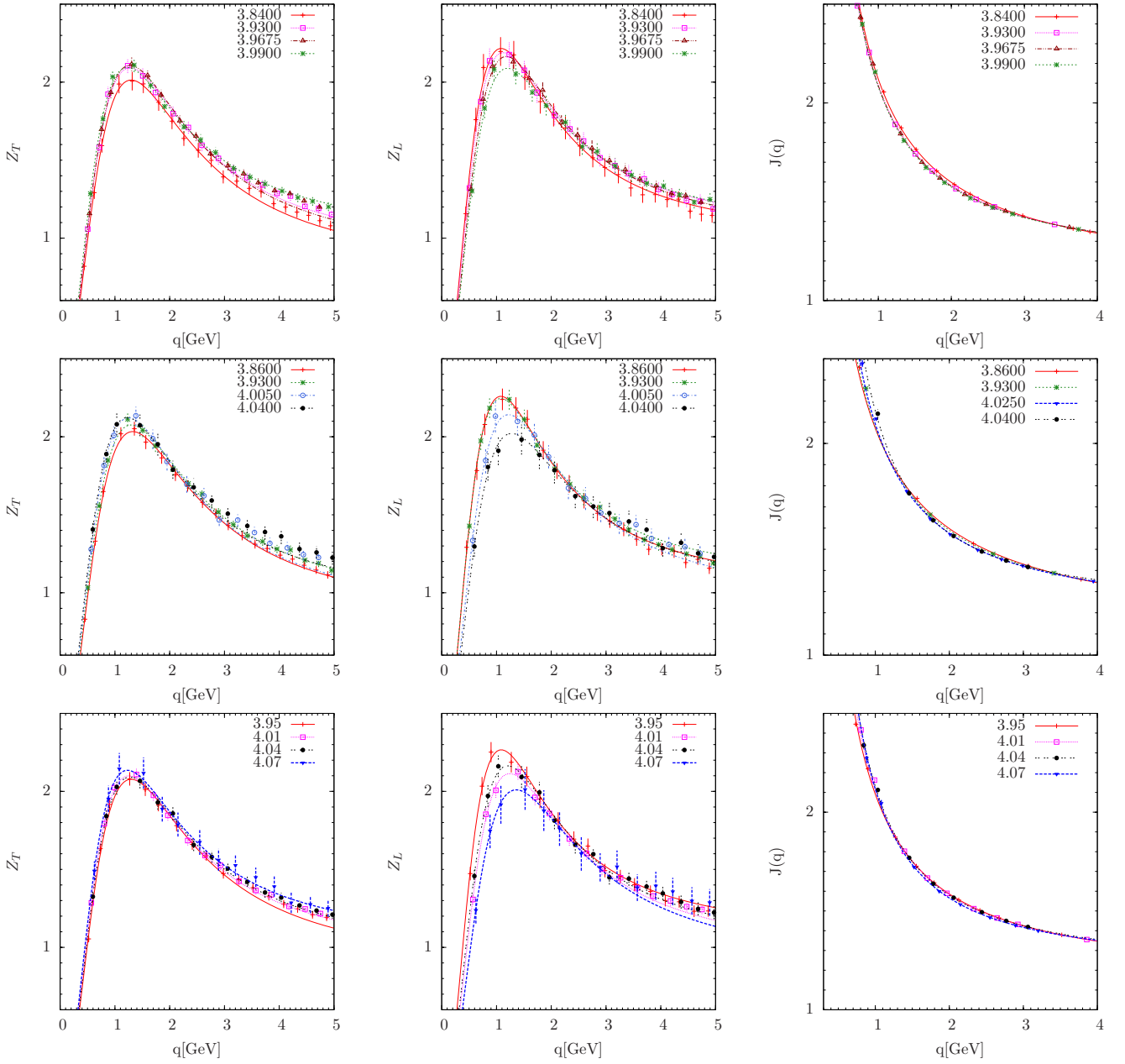


FIG. 1: The unrenormalized dressing functions for the transverse gluon  $Z_T$  (left panel), for the longitudinal gluon  $Z_L$  (middle panel) and for the ghost dressing function  $J$  (right panel) are shown as functions of the momentum  $q$  [GeV] for different (inverse) coupling values  $\beta$  (i.e. different temperatures) given in the legend. The corresponding pion mass values (from top to bottom panels) are  $m_\pi \simeq 316, 398, \text{ and } 469$  MeV.

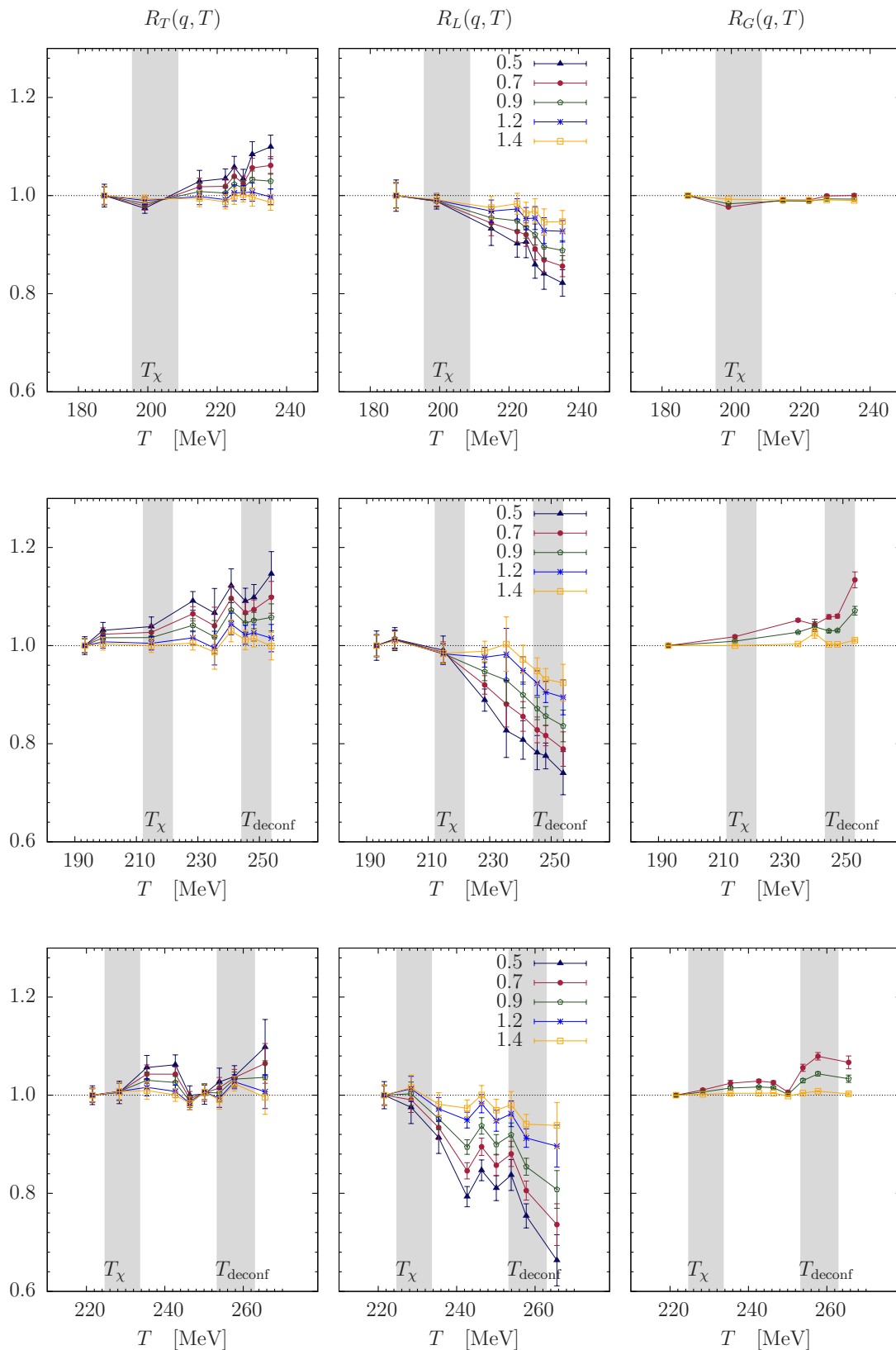


FIG. 2: Ratios  $R_T$ ,  $R_L$  and  $R_G$  for the renormalized transverse  $D_T^{ren}$  (left panel), longitudinal  $D_L^{ren}$  (middle panel) and ghost  $G^{ren}$  (right panel) propagators, respectively, as functions of the temperature  $T$  at a few non-zero momentum values  $q$  (indicated in units of [GeV]). The corresponding pion masses (from top to bottom) are  $m_\pi \simeq 316$ , 398 and 469 MeV. The vertical bands indicate the chiral and deconfinement pseudo-critical temperatures with their uncertainties (see Table II).

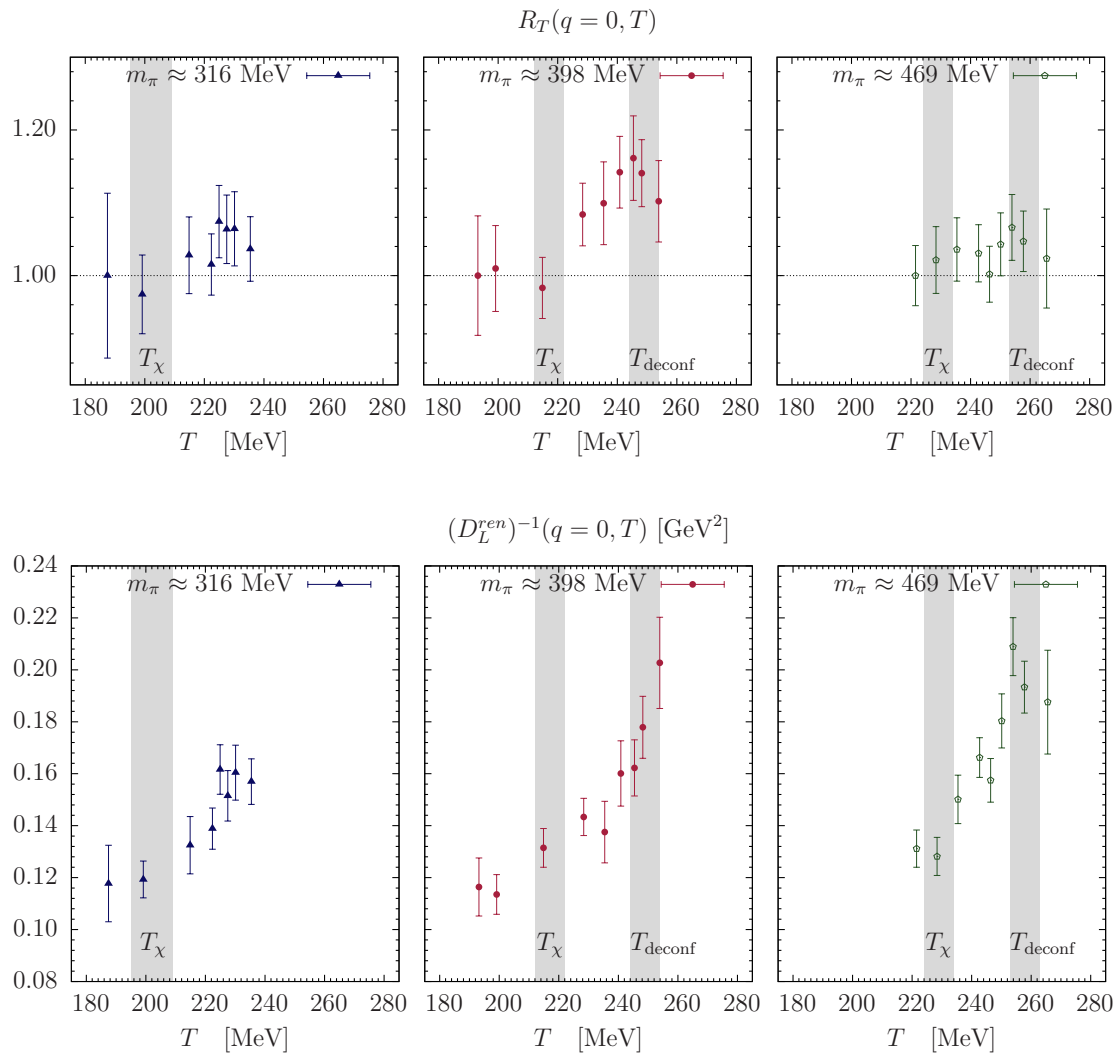


FIG. 3: The upper row shows the ratio  $R_T$  at zero momentum for the three pion mass values indicated. The lower panels show the inverse renormalized longitudinal gluon propagator  $(D_L^{ren})^{-1}$  at zero momentum.